Light Metals 2013 *Edited by: Barry Sadler*
TMS (The Minerals, Metals & Materials Society), 2013

MICROSTRUCTURAL EVOLUTION OF CAST IRON USED FOR CATHODE RODDING IN ALUMINIUM ELECTROLYSIS CELL

Alireza Hekmat-Ardakan[1], Gervais Soucy[1], Loig Rivoaland[2]
[1] Department of Chemical Engineering and Biotechnological Engineering, Université de Sherbrooke, J1K 2R1, Canada
[2]Rio Tinto Alcan (Centre de Recherche et Développement d'Arvida), P.O. Box 1250, Jonquière, Québec, G7S 4K8, Canada

Keywords: Aluminum, Electrolysis, Cast iron, Collector bar

Abstract

The microstructure of cast iron sealed to the steel collector bar through casting process was investigated using optical and scanning electron microscopes equipped with an energy-dispersive X-ray (EDX) analyzer in as cast condition and after 3 and 9 hours electrolysis tests in laboratory scale. Thermodynamic study was also carried out using Factsage software and the results were compared with DSC (Differential Scanning Calorimetry) test to reveal the solidification behavior of the cast iron. The microstructural observation indicated a significant change particularly at the interface of cast iron-steel after the electrolysis tests due to the time dependent diffusion of the elements, mainly carbon and phosphor, from cast iron into the steel. The diffusion zone inside the steel collector bar with pearlitic microstructure can be visually detected and separated from the regular (non diffused) ferritic steel by etching the metallographic samples using Nital reagent.

Introduction

In order to save a massive amount of energy during the production of aluminum, any electrical resistance must be minimized from the current path as far as possible. This includes the electrical resistance made from the casting of the high phosphorous gray iron (HPGI) as a sealant between the carbon or graphite cathode and the steel collector bar. Although the electrical resistivity can partly be affected by the type of cast iron, its contact resistance with the steel collector bar as well as with the cathodic block plays a more important role. However, it is worth noting that the type of cast iron and more attentively, its chemical composition, influence the contact pressure particularly during the cell startup.

In this study, the focus will be put on the microstructure at the interface of HPGI-Steel collector bar in as cast and after laboratory electrolysis process. Thermodynamic calculations are also carried out using Factsage thermochemical software and database [1] to predict the solidification behavior of HPGI in both equilibrium and non-equilibrium (Scheil) cooling conditions. The results are then compared with DSC (Differential Scanning Calorimetry) tests at constant cooling and heating rate of 10 $^{\circ}$C min^{-1}. The thermal expansion coefficient measurement of HPGI with the same heating rate used for the DSC test is carried out to correlate the detected peaks with the Factsage predictions as well as DSC measurements.

Factsage thermodynamic calculation

HPGI provided from RTA was used in this study. High phosphor amount makes the molten HPGI more fluid during the casting process as a result of its action to reduce its freezing point [2] while decreasing the electrical conductivity of the alloy. It is also an undesirable impurity in the aluminum reduction process with a detrimental effect on current efficiency (CE) of the process when it enters in cryolite-alumina melt in the form of phosphate anion [3]. It was reported that 100 ppm of phosphor enables to reduce the CE by 1 % [3]. However, the cathode cast iron is not in direct contact with the bath except at the very end of life of the electrolysis cell. Consequently, phosphorous contamination of the aluminum is not reported, and phosphorous can be advantageously added to the cast iron used for sealing the cathodic collector bars (but not for the anode rodding, since the anode stubs can be in contact with the bath, from time to time).

Figure 1 depicts the isopleths diagram of Fe-C-3.2 % Si-1.5 % P-0.5 % Mn (wt %). The dashed line shows the solidification behavior of HPGI at 3.4 % C implying the start and the end of the solidification at 1 412 °C and 1 000 °C, respectively. In fact, the solidification becomes terminated by precipitation of iron phosphide (Fe_3P) phase at an isothermal eutectic reaction in equilibrium state. Therefore, the addition of phosphor enables to reduce the endpoint of solidifying temperature down to 1 000 °C [4]. With further reduction of temperature, the phase changes in solid state, mainly eutectoid reaction of austenite (γ) → ferrite (α) + cementite (Fe_3C) takes places at 822 °C and pearlitic matrix forms.

Figure 2 compares the solidification amount of HPGI as a function of temperature for equilibrium and non-equilibrium (at 10 and 15 °C min^{-1}) cooling conditions. No difference is observed between the cooling curves up to almost 50 % of liquid fraction. By continuing solidification of alloy, non equilibrium cooling curves indicate more liquid fraction compared to the equilibrium cooling curve resulting in lowering the end of solidification temperature down to 960 °C as shown by arrows.

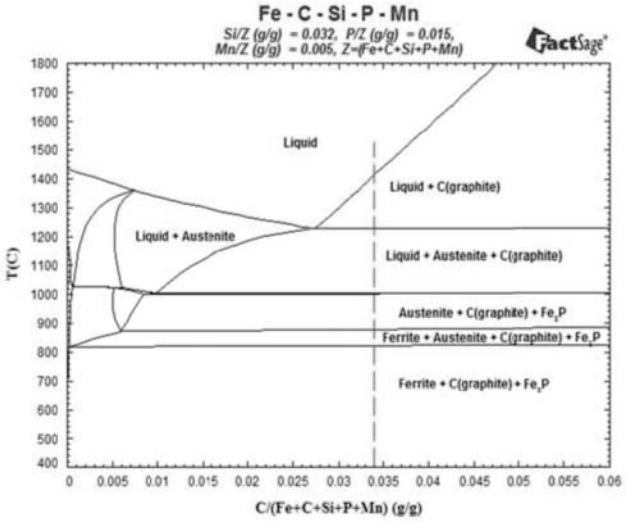

Figure 1: Solidification path of HPGI calculated by Factsage.

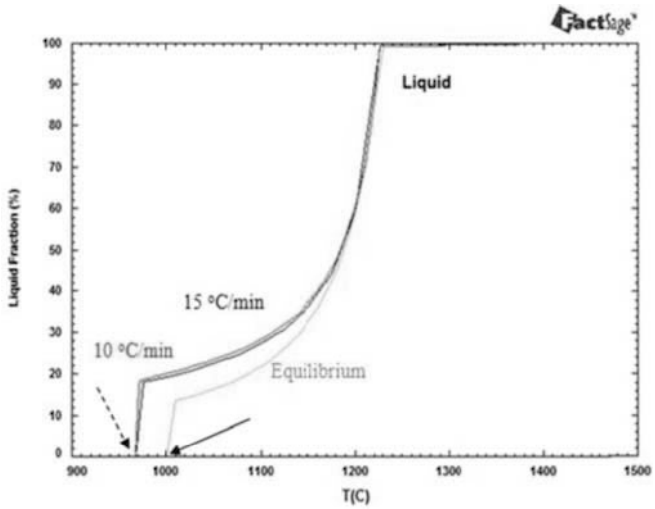

Figure 2: Comparison of solidification amount of HPGI for different cooling rate

In order to validate the results obtained from the thermodynamic calculations for the solidification of HPGI, DSC test was carried out on HPGI samples during heating and cooling process as shown in Fig.3. DSC measurement clearly shows that the melting temperature of HPGI begins at about 988 °C while its solidification ends at about 926 °C. Delay in solidification ending temperature compared to the start of melting arises from the undercooling effect required for solidification [5]. Nevertheless, the Factsage calculations indicate the solidification ending temperature about 35 °C higher than that of DSC experiment.

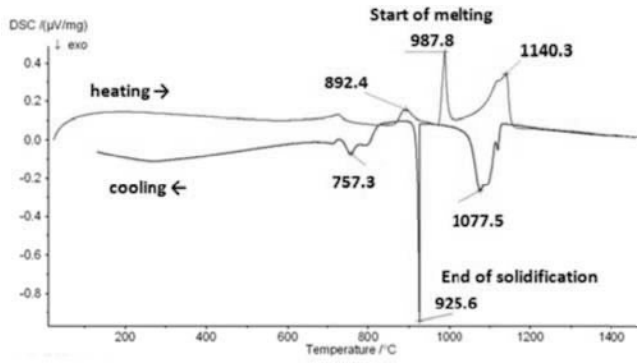

Figure 3: DSC measurement in cooling and heating of HPGI at the rate of 10 °C min^{-1}

Figure 4 shows the thermal expansion test of HPGI carried out to justify the identified peaks in DSC test during heating process. It is clearly observed that the HPGI sample expands with a constant rate by increasing temperature up to 873.1 °C (892.4 °C at DSC test) where a contraction occurs [6] as a result of the iron phase change from ferrite (α) to austenite (γ). Subsequently the alloy continues to expand for a second time up to 977.8 °C. With further increase of the temperature, the expansion graph abruptly declines unlike other ferrous alloy with low phosphor content. This is indeed the point that the alloy begins to melt as shown in DSC test at 987.8 °C. The expansion measurement will not be valid for the temperatures higher than this point due to the melting of phosphorous content phase of Fe_3P.

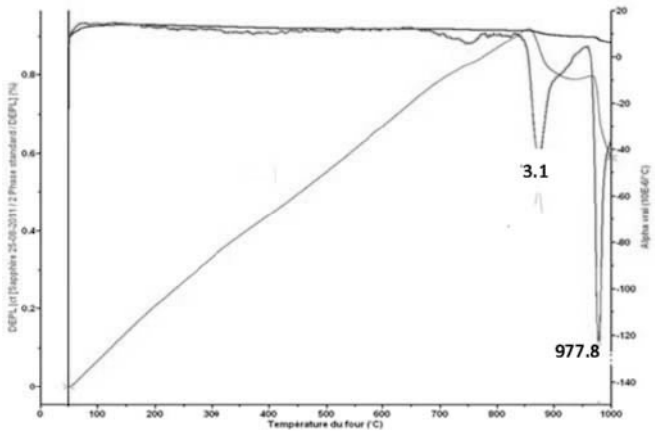

Figure 4: Thermal expansion coefficient of HPGI vs. temperature graph indicates an irregular reduction in expansion at 977.8 °C due to the melting of Fe_3P phase.

As cast rodding microstructure

Rectangular graphitic block (120 mm × 75 mm × 200 mm (LWH)) with a slot size 20 mm × 20 mm machined at the bottom surface was used for electrolysis tests. Steel collector bar was machined to 10 mm × 10 mm and was centered in the slot using ceramic plates. The entire block with collector bar was then put in a heat treatment furnace to be preheated at 400 °C before casting. The effects of preheating temperature and the methods applied in industrial conditions play a significant role in final microstructure of rodding cast iron and particularly in the contact pressure (thermal stress) made on cathodic block during the cell start-up. However this subject is beyond the scope of this study and much research is needed to investigate this effect. HPGI alloy was melted by induction furnace and poured into slot already preheated. Metallographic sample cut from the center of bar was polished and etched by Nital reagent (a solution of 4 % acid nitric and 96 % alcohol) to investigate the microstructure at HPGI-bar interface in as cast condition.

Figure 5a shows the microstructure at the interface HPGI-bar casting process. Figure 5a indicates that the rapidly cooled microstructure of HPGI is mainly similar to the white cast iron [7] containing cementite (Fe_3C), very fine pearlite and a network of iron phosphide (Fe_3P) as depicted in Figure 5b.

However, the precipitation of graphite inside the HPGI region with ferritic microstructure was also observed only near to the interface of HPGI-steel as shown in Figs. 5a and 6. On the other side of the interface, inside the steel region with a typical ferritic microstructure, a layer about 70 microns containing fine pearlitic microstructure was detected near to the interface. This phenomenon may occur due to the diffusion of carbon from HPGI into the steel forming ferritic and pearlitic microstructures on both HPGI and Steel sides of the interface, respectively.

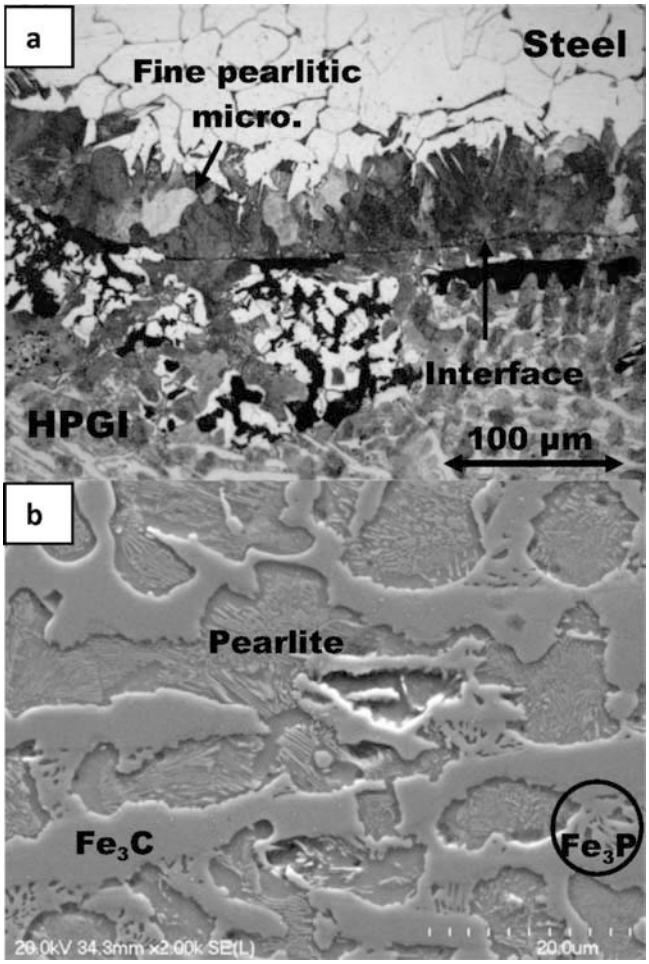

Figure 5: (a) Microstructure at the Interface of HPGI-Steel bar after casting and (b) white cast iron microstructure of at the center of HPGI away from the interface

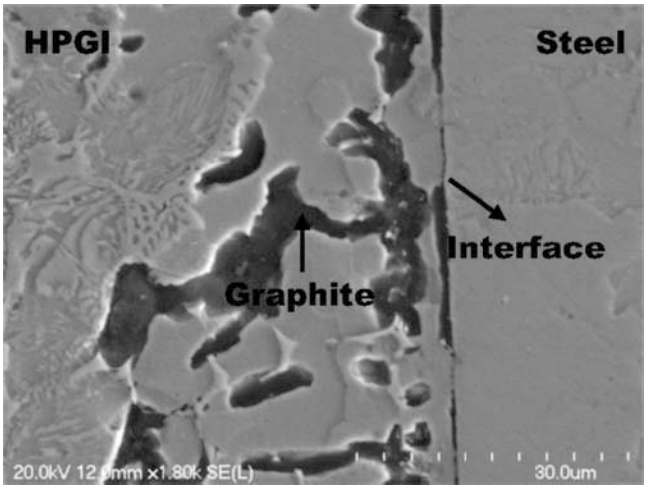

Figure 6: Precipitation of graphite with ferritic matrix near to the interface while the rest of HPGI is white cast iron.

Microstructure after electrolysis tests

Two electrolysis tests were separately carried out for 3 and 9 hours at 960 °C using the graphitic blocks with sealed HPGI. RTA cryolitic electrolyte was used for the tests. The detail of the electrolysis process can be found in our previous TMS publication [8]. After electrolysis tests, the cast iron attached to the bar was removed from the block and a sample for metallographic purpose was cut at the center of the bar. Figure 7 compares the metallographic surface of HPGI-bar etched by Nital reagent after two electrolysis tests. The layer formed around the bar and pointed by arrows in Figure 7 shows the zone where carbon diffuses from HPGI into the steel bar. This layer appears immediately after etching the surface with Nital reagent. It is clearly observed that the carbon diffusion layer becomes thicker (1.3 mm and 2.6 mm, respectively) with electrolysis time as expected.

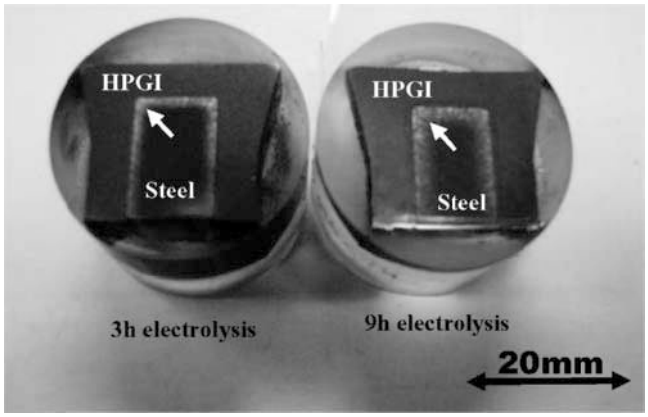

Figure 7: Nital etched metallographic surface of HPGI-steel bar after two electrolysis test, arrows point to the diffusion layer.

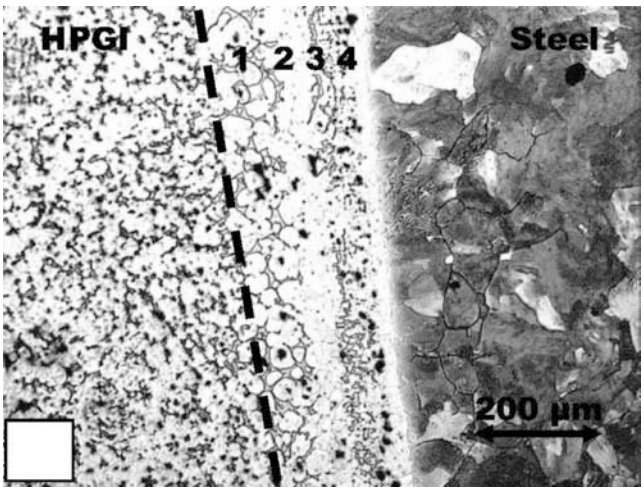

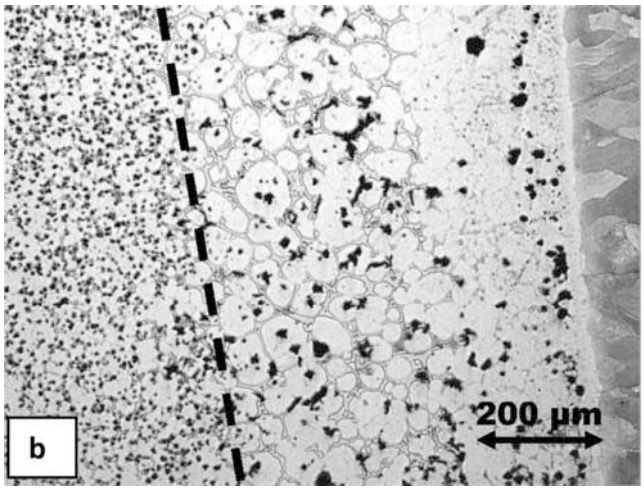

Figure 8: Microstructure of HPGI after electrolysis for (a) 3hrs and (b) 9hrs showing the width of diffusion layer.

Figure 8 shows the microstructure of HPGI-steel bar after two electrolysis tests. The microstructure of HPGI contains irregular form of graphite precipitated from decomposition of cementite existing in as-cast microstructure dispersed in a ferritic matrix as well as a network of phosphor containing phase. The microstructure of HPGI close to the interface where carbon migrates toward steel is quite different compared with the rest of HPGI microstructure as shown in both Figure 8a and 8b with dashed lines. Graphite size in this layer is extremely bigger than those out of the layer. Phosphor also diffused to this layer and made a large and interconnected network of Fe_3P particles. Figure 8a demonstrates that this layer can be divided into 4 regions in terms of Fe_3P distribution. Large Fe_3P particles are observed in the first region. In the second region, there is only ferritic matrix without presence of any Fe_3P particle. Third region once more shows the Fe_3P particles but fairly smaller than those in the first region. In the last region only ferritic matrix is again observed. It is worth noting that the original interface position must be situated right next to the most distal graphite particles at the left side of the region 4 as shown in Figure 8 while the pearlitic microstructure has been formed at the other side of the region 4. By close attention to this region using a SEM image shown in Figure 9, it is observed that the HPGI-steel collector bar interface has been completely disappeared implying the integration of both alloys.

By comparing Figure 8a and 8b, it is also observed that the thickness of the diffusion layer after 9hrs electrolysis test which reaches about 700 µm is at least three times bigger than of 3 hrs. Moreover, there are no Fe_3P particles in the third region for higher electrolysis time as shown in Figure 8b.

As it was mentioned in Figure 7, large pearlitic zone forms inside the steel bar due to the diffusion of carbons from the HPGI layer shown in Figure 8. It is interesting to note that the diffusion of P element into the steel was also detected for both samples.

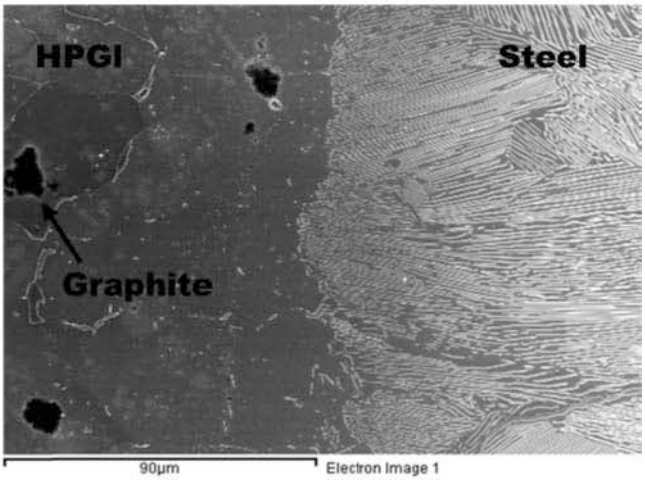

Figure 9: HPGI and steel are integrated together after both electrolysis tests without having interface.

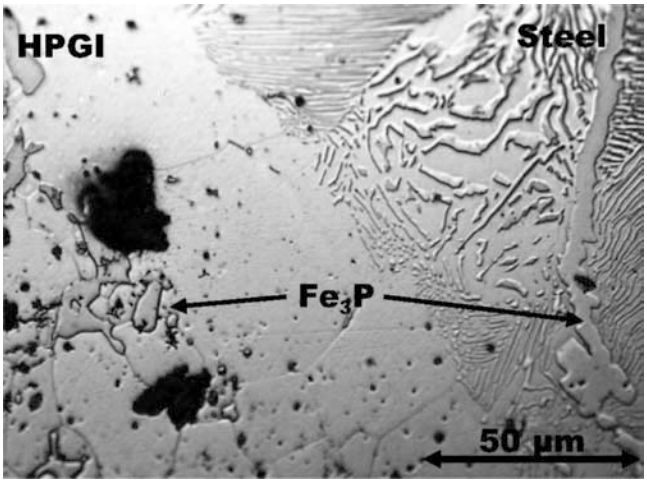

Figure 10: Diffusion of P into the pearlitic layer of steel after 3hrs electrolysis test.

Figure 10 shows the diffusion of P in the pearlitic layer of the steel bar at the interfac position after 3hrs electrolysis. It is therefore concluded that both C and P elements diffuse from HPGI into the steel collector bar forming a particular layer in both HPGI and steel bar alloys close to their interface. However the diffusion of C is more significantly deeper than the P into the steel.

Labrecque et al. [6] have also investigated the microstructure of both HPGI rodding and steel collector bar before (as-cast) and after the period of electrolysis operation in the plant. They characterized the microstructure of as-cast HPGI as white cast iron without pointing out the microstructure at the interface HPGI-Steel.

After service, they showed the interface microstructure containing the integration of both metals (disappearance of interface) as well as the formation of phosphide parallel to the interface due to the diffusion of phosphor element. They have also pointed to some cavities planes formed at the interface. However the goal of their study was to compare two different types of cast iron i.e. HPGI and FDI (ferritic ductile iron). They have not sophisticatedly characterized the microstructure before and after electrolysis process.

Conclusions

The study of solidification behaviour of HPGI (high phosphorous gray iron) used as a rodding of cathode to the steel collector bar showed the decrease of the freezing point down to about 960 °C and 925 °C according to the Factsage calculation and DSC measurement, respectively. The thermal expansion test also confirmed the melting temperature of HPGI at about 978 °C (988 °C by DSC test) by the abrupt decline of the expansion vs. temperature graph.

The microstructure at the interface of the cast HPGI and steel collector bar was also studied in as-cast and after 3 and 9 hrs electrolysis tests. The rapidly cooled microstructure of HPGI was mainly white cast iron containing cementite (Fe_3C), very fine pearlite and a network of iron phosphide (Fe_3P) except at the interface where graphitization has occurred. A diffused carbon layer with a width of about 70 microns containing pearlitic microstructure was detected around steel side of the interface.

After 3 and 9 hrs electrolysis tests, a layer was formed next to the interface position of both HPGI and steel due to the diffusion of carbon. A layer with the microstructure entirely formed from the fine pearlite was detected at the interface of the steel with ferritic microstructure. This layer can be visually observed on the surface of the metallographic samples right after the etching process by Nital in the form of a white layer. The thickness of the layer was measured to be 1.3 mm and 2.6 mm respectively. The layer formed at the interface of HPGI had a width respectively about 220 µm and 700 µm containing bigger graphite with less particle fraction in comparison to the graphite particles out of the layer. On the other hand, extremely large and interconnected network of Fe_3P particles was observed in this layer. After electrolysis tests, the interface line of HPGI-steel observed in as-cast microstructure was completely disappeared and both alloys were integrated together. This phenomenon facilitates the current passing through the interface during the electrolysis process.

Acknowledgement

This work was made possible with financial participation of Rio Tinto Alcan (RTA), "Conseil de Recherches en Sciences Naturelles et en Génie du Canada" (CRSNG) and "Fonds Québécois de la Recherche sur la Nature et les Technologies" (FQRNT). Authors gratefully acknowledge the personnel of "Centre de Caractérisation des Matériaux", at Université de Sherbrooke for material characterization.

References

1. C. W. Bale, E. Bélisle, P. Chartrand, S. A. Decterov, G. Eriksson, K. Hack, I. H. Jung, Y. B. Kang, J. Melancon, A. D. Pelton, C. Robelin, S. Petersen, ¨FactSage thermochemical software and databases - recent developments¨, *Calphad: Computer Coupling of Phase Diagrams and Thermochemistry* 2009, *33* (2), 295-311.

2. John Campbell, *Complete Casting Handbook* (Butterworth Heinemann, Elsevier, 2011), 1220 p.

3. M. Keppert, G. M. Haarberg and S. Rolseth, ¨Electrochemical behavior of aluminum phosphate in cryolite-alumina melts¨ *Proceedings-Electrochemical Society,* PV 2004-24 (2006), 237-245.

4. V. Raghavan, ¨C-Fe-P (Carbon-Iron-Phosphorus), ¨*Journal of Phase Equilibria and Diffusion*¨, *25* (6), (2004), 541-542.

5. J. R. Davis, *Cast Irons.* (ASM International: Technology & Engineering, 1996), 494 p.

6. L. Caruso, K. A. Rye, and M. Sorlie, ¨Experimental comparison of cathode rodding practices¨, *TMS Light Metals*, The Minerals, Metals and Materials Society, (2007), 827-831.

7. C. Labrecque, M. Gagné, D. Lavoie, A. Lévesque, and B. Murphy, ¨A new technology for cathode rodding used in aluminium electrolytic cells, *TMS Light Metals*, The Minerals, Metals and Materials Society, (2003), 661-667.

8. M. Brassard, M. Lebeuf, A. Blais, L. Rivoaland, M. Désilets and G. Soucy, ¨Characterization of carbon cathode materials by X-ray microtomography¨, *TMS Light Metals*, The Minerals, Metals and Materials Society, (2012), 1325-1329.